ELSEVIER

Journal of Alloys and Compounds 275–277 (1998) 161–169

Journal of ALLOYS AND COMPOUNDS

NMR spectroscopy of rare earth–3d transition metal alloys

Czesław Kapusta*

Department of Solid State Physics, Faculty of Physics and Nuclear Techniques, University of Mining and Metallurgy, 30-059 Kraców, Poland

Abstract

Recent nuclear magnetic resonance studies of magnetically ordered rare earth–3d transition metal alloys are reviewed. Selected experimental results for rare earth NMR of $RETM_2$ Laves phases as well as $RE_2TM_{14}B$ and interstitially modified $RE_2TM_{17}A_x$ (A=N,C,H) materials for permanent magnet applications are surveyed. An analysis of the hyperfine parameters obtained from NMR experiments is presented and their relation to the physical properties of individual atomic sites is discussed. In particular, information from hyperfine fields about the influence of light interstitial atoms on the RE–TM magnetic coupling is analysed and compared to the results of magnetisation and neutron measurements. The relation of quadrupole splitting to the spectroscopic state of the rare earth, the magnetic structure and the individual site contributions to the magnetocrystalline anisotropy is analysed. The applicability of NMR to the study of multiphase magnetic materials for technology is briefly discussed. © 1998 Elsevier Science S.A.

Keywords: Hyperfine fields – magnetic; Intermetallic compounds; Magnetocrystalline anisotropy; NMR – spin echo; Quadrupole interactions

1. Introduction

Rare earth–3d transition metal (RE–TM) compounds exhibit a variety of interesting structural and magnetic properties which make them attractive for novel material science. Most of their crystallographic structures contain several sublattices, so the intrinsic parameters of the compounds are products of individual site contributions. Thus, knowledge of individual site properties is vital for a correct description of their fundamental properties, as well as for desirable modification of their parameters essential for applications. Information on the individual sites can be obtained in nuclear magnetic resonance (NMR) from the hyperfine parameters reflecting the interaction of the spin and quadrupole moment of a nucleus with magnetic fields and electric field gradients (EFG) produced by unfilled electron shells and neighbouring ions. The polarisation of electronic shells in an applied magnetic field or exchange molecular field is different for inequivalent sites and results in a difference of magnetic hyperfine fields (HFF) and EFG between the sites. From these data information on the site environments, magnetic moments and their coupling, as well as the contributions to the magnetocrystalline anisotropy can be derived.

Nuclei with nonzero spin can serve as probes for magnetic fields, whereas those with spins $I>1/2$ having nonvanishing quadrupole moments can also probe EFG, so the majority of isotopes in the Periodic Table can be used as NMR probes. For general information on the basic principles of NMR see Ref. [1]. The specific requirements of the experimental technique and the information obtained depend on the materials investigated. For example, features of classical NMR in diamagnetic materials [2] are different from those of the frequency-swept spin-echo NMR in strongly magnetic materials [3–6].

In $RE_2TM_{17}A_x$, $RE_2TM_{14}B$ and $RETM_2$ (TM=Fe or Co) compounds, which will be discussed here, a strong exchange interaction of the 3d metal sublattice gives rise to a high Curie temperature and saturation magnetisation. The rare earth element is responsible for the magnetocrystalline anisotropy through the interaction of its aspherical 4f electron shell with the crystalline electric field (CEF). The TM–RE exchange interaction arises from 3d–5d hybridisation and corresponds to an antiparallel coupling of 3d TM and 5d RE spins. The intraatomic exchange couples 4f and 5d spins ferromagnetically which results, for light (heavy) RE, in a parallel (antiparallel) coupling of the 4f magnetic moment with the 3d TM moment.

Most of the NMR measurements discussed here were carried out at 4.2 K to profit from the large paramagnetic nuclear magnetisation and the slow nuclear relaxation

*Fax: +48 12 6341247; e-mail: kapusta@uci.agh.edu.pl

0925-8388/98/$19.00
PII: S0925-8388(98)00295-3

resulting in a relatively large NMR signal at low temperatures. Polycrystalline powder samples were used.

2. NMR of magnetically ordered materials

The characteristic features of NMR for magnetically ordered materials are related to the presence of internal fields resulting from the magnetic order. Thus, the resonant condition can be fulfilled at zero applied magnetic field making use of the effective internal field B_e at the nucleus. If the quadrupole interaction is much smaller than the magnetic interaction, the resonant frequencies, to a first-order approximation, are given by the relation

$$\nu_{m,m-1} = |\gamma_n B_e/2\pi + P_q(2m-1)|, \quad (1)$$

where m runs in integer steps from $1-I$ to I and γ_n is the gyromagnetic constant relating the resonance frequency to the field at the nucleus. P_q is the quadrupole parameter. The internal magnetic field B_e at a nucleus can be expressed as follows:

$$B_e = B_{loc} + B_{hf} \quad (2)$$

where B_{loc} is the local field consisting of the Lorentz field and the dipolar field B_{dip}, which is usually the dominant contribution to B_{loc}. B_{dip}, however, rarely exceeds 1 T. The hyperfine field B_{hf} is usually the dominant contribution and B_e is sometimes called synonymously ''hyperfine field'' and abbreviated HFF. B_{hf} can be expressed as a sum:

$$B_{hf} = B_s + B_{orb} + B_n \quad (3)$$

where B_s is the self polarisation term originating from core and conduction electron polarisation by the spin moment of the parent atom. B_{orb} is the orbital field produced by nonvanishing orbital moments of the 4f electrons and is dominant for the non-S-state rare earths. B_n is the polarisation contribution from neighbouring magnetic atoms often called the ''transferred'' HFF. The contributions to HFF are related to the constituents of the magnetic moment through the hyperfine coupling and can be written as $B_i = A_i \times \mu_i$, where i stands for indexes ''s'' and ''orb''.

For a nucleus with $I > 1/2$ and a ''small'' quadrupole interaction, i.e. with $2mP_q \ll \gamma_n B_e$, the spectrum has the form of $2I$ equidistant lines. From the quadrupole splittings $\Delta\nu_q$ derived from the line separations of the quadrupole spectra the corresponding values of the EFG component along the hyperfine field V_{ii} can be derived using the formula

$$|V_{ii}| = 2I(2I-1)h\Delta\nu_q/3e|Q_n| \quad (4)$$

where Q_n is the nuclear quadrupole moment.

The EFG at the nucleus of a non-S-state rare earth originates mainly from the nonspherical distribution of the 4f electron density of the parent ion as well as from the asphericity of the 6p and 5d electron density of the parent ion due to the presence of neighbouring atoms in the lattice [7]. Thus, the diagonal EFG component along the hyperfine field direction may be written as

$$V_{ii} = V_{ii}(4f) + V_{ii}(latt) \quad (5)$$

In compounds where the RE–TM exchange interaction is much stronger than the crystal electric field interaction, e.g. in $RETM_2$ or $RE_2TM_{17}A_x$, where TM = Fe,Co and A = N,C,H, the rare earth usually preserves its fully polarised ground state with $J_z = J$ irrespective of the direction of magnetisation. Thus, $V_{ii}(4f)$ is independent of the magnetic moment direction and has its maximum value denoted as $V_{zz}(4f)$, which is proportional to the quantum number J_z. Also, B_{orb} preserves its maximum value.

The complete spectrum of a nucleus, such as ^{147}Sm, very often covers a range corresponding to a few hundred MHz, so the most useful technique is frequency-swept spin-echo NMR at zero applied field. A standard two-pulse sequence of radiofrequency (rf) pulses is usually applied and the amplitude of the nuclear spin echo appearing after the second pulse after a time equal to the pulse separation is measured. An external magnetic field can be applied for saturation of the sample or determination of the origin of an unknown signal. Recent progress in broadband rf electronics has allowed the construction of an untuned, 10–1000 MHz, computer controlled frequency-swept spectrometer [8] and made NMR research of magnetic materials much more effective.

The presence of a magnetic domain structure in ordered materials leads to enhancement of the rf field and lowers the pulse power required to form a spin echo. The enhancement effect is caused by oscillations of the electronic magnetisation excited by the rf pulses. A rf field enhanced through the hyperfine coupling appears at the nucleus. The effect is much larger in the domain walls than in domains so the signals from domain walls are usually observed. The rf enhancement varies across the domain wall and is larger at the domain wall centre (DWC) than at the domain wall edge (DWE). Thus, the DWC signals can be distinguished from the DWE signals on the basis of their dependence on the rf pulse power. The maximum of the former usually corresponds to a much lower pulse power than that for the latter. For large enough power we can study DWE regions adjacent to domain interiors, where the directions of magnetic moments are nearly parallel and are representative of the direction of the moment in the domain interior. It is essential to obtain a signal corresponding to a well defined direction of local magnetisation with respect to the crystallographic axes when we study anisotropic properties such as EFG and orbital contributions to magnetic moments. Another possibility to distinguish between DWC and DWE signals is related to the difference of their nuclear relaxation rates. Since the relaxation of the DWC signal is much faster than the DWE signal, measurement at large pulse separation removes the DWC signal but leaves the DWE signal.

A feature of zero applied field NMR worth noting is that the spectrum depends on the mutual directions of B_e, which usually follows the local magnetisation, and the principal axes of the EFG tensor, which are rigidly coupled to the crystal lattice. The spectra of polycrystalline samples are therefore equivalent to those of single crystals.

3. $RETM_2$

The Laves phase compounds $RETM_2$ (TM=Co,Fe) exhibit interesting physical properties related to the interplay of the itinerant magnetism of Co(Fe) 3d electrons and the localised magnetic moments of the rare earth. Magnetic phenomena in these compounds include a giant, anisotropic magnetostriction related to the single ion interaction due to the influence of the crystalline electric field on the rare earth ion [9]. An example of such behaviour is $SmCo_2$. This compound shows a cubic crystal lattice at room temperature with single crystallographic sites for Sm and Co. It orders ferromagnetically at 259 K and undergoes a rhombohedral distortion of its cubic crystal lattice at 210 K. The easy magnetisation direction (EMD) of the compound has been determined by a ^{59}Co NMR study [10] to lie along the ⟨111⟩ crystallographic axis. It causes the appearance of two resonance lines in the ^{59}Co spectrum. The relative intensity ratio of approximately 3:1 is in agreement with the population ratio of the two magnetically inequivalent Co sites. Ref. [11] reports a ^{147}Sm and ^{149}Sm (nuclear spins $I=7/2$) NMR study at 4.2 K in the distorted phase.

The ^{147}Sm spectrum shown in Fig. 1 consists of three septets, one at high frequency and two at low frequency, and is consistent with the spectrum of ^{149}Sm, which has a three times smaller quadrupole splitting corresponding to the three times smaller nuclear quadrupole moment of ^{149}Sm. The frequencies of the central lines correspond to values of B_e at Sm nuclei of 320.3 T (central frequency 563.1 MHz), 320.4 T (central frequency 563.3 MHz) and 342.3 T (central frequency 601.8 MHz) for the three septets. The quadrupole splittings ν_q obtained from the line separations within the septets amount to 9.4, 10.5 and 7.0 MHz, respectively. Using the conversion factor -21.85×10^{20} V/m^2 MHz assuming the dominant, negative contribution from the 4f electrons, the values of the EFG component along the direction of B_e have been derived. They amount to -205.4×10^{20}, -229.4×10^{20} and -153.0×10^{20} V m^{-2}, respectively. Subtracting the value of the 4f electron contribution of -240×10^{20} V m^{-2} as determined for Sm_2Co_{17} [12], the component of the lattice contribution along B_e has been evaluated at 34.6×10^{20}, 10.6×10^{20} and 87.0×10^{20} V m^{-2}.

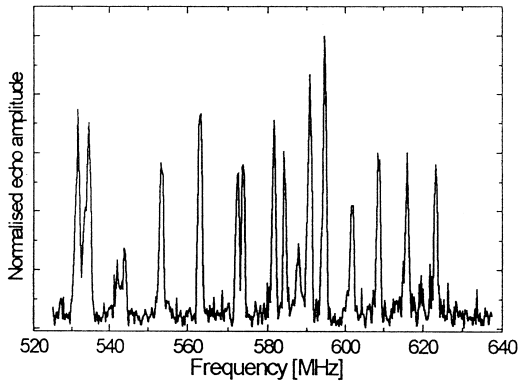

Fig. 1. ^{147}Sm spin-echo NMR spectra of $SmCo_2$ at 4.2 K (after Ref. [11]).

Sharp resonance lines with well defined quadrupole splittings are related to unique directions of magnetic moments, i.e. with domain wall edges, rather than with domain wall centres, where a spread of quadrupole splittings and hyperfine fields is expected. For the EMD along the ⟨111⟩ axis in the rhombohedrally distorted lattice, we expect two magnetically inequivalent Sm sites, one with its moment along the direction of puckering of the cube, ⟨111⟩ (the 0° site) and the other along the directions ⟨11−1⟩, ⟨1−11⟩ and ⟨−111⟩ (the 70.5° site). The relative population of these sites should be 1:3. On this basis the upper septet could be attributed to the 0° site and the two low frequency septets to the 70.5° sites. The presence of two septets corresponding to the 70.5° site indicates its further splitting into two inequivalent sites.

A considerable value of the lattice EFG indicates that the second-order term of the crystalline electric field interaction with the 4f electronic shell, i.e. interaction of the EFG with the quadrupole moment of the 4f shell, becomes important in the rhombohedrally distorted structure. From the value of the lattice EFG along the ⟨111⟩ direction (site 0°), a crystalline electric field coefficient A_2^0 of $-221\,Ka_0^{-2}$ was obtained under the assumption of an approximate proportionality between the lattice EFG at the nucleus and the crystalline electric field coefficient A_2^0 [7]. A proportionality factor of $-2.54\times10^{-20}\,Ka_0^{-2}$/V m^{-2}, derived from a comparison of bulk anisotropy measurements and lattice EFG derived from Mössbauer measurements on various rare earth–3d metal compounds [13], has been used.

4. $RE_2TM_{17}A_x$

The host compounds crystallise in the rhombohedral structure for the light rare earths and in the hexagonal structure for Y and the heavy rare earths. The reaction of RE_2TM_{17} with N_2, NH_3, C_2H_2, CH_4 or H_2 gases to form interstitial nitrides, carbides and hydrides, preserves the structure of the parent materials. Both structures contain four inequivalent TM sites denoted 12k, 12j, 6g and 4f in the hexagonal form, which correspond to 18h, 18f, 9d and 6c, respectively, in the rhombohedral compound. RE

elements occupy a single site, 6c, in the rhombohedral and two sites, 2b and 2d, in the hexagonal structure. Neutron diffraction experiments have shown that in the interstitial carbides prepared from a melt the C atoms randomly occupy the interstitial positions 9e (6h) [14]. The hydrogen atoms locate at 9e and 18g (6h and 12i) sites. The 9e (6h) sites can be completely filled, whereas a maximum of only one-third of the total number of the 18g (12i) sites can be occupied, which leads to a maximum content of interstitial hydrogen, $x=5$ [15]. Nitrogen locates entirely at 9e (6h) interstitial positions to a maximum content of $x=3$ in the formula $RE_2TM_{17}N_x$ when prepared in a N_2 gas atmosphere [16]. For hydrogen pre-treated samples nitrided in ammonia a nitrogen content of 4 was reported [17]. In such a material, the location of some N atoms at the 18g (12i) sites in addition to the 9e (6h) site occupation was concluded from neutron diffraction measurements [18,19]. The number of 9e (6h) and 18g (12i) nearest neighbour (NN) positions to RE sites is 3 and 6, respectively. Information on the structural and magnetic properties of interstitial nitrides, carbides and hydrides can be found in review papers [20,21].

4.1. ^{89}Y resonance

NMR spectra measured on $Y_2Fe_{17}C_x$ samples prepared by co-melting appropriate amounts of the constituents have been reported [22]. The spectra, shown in Fig. 2, consist of

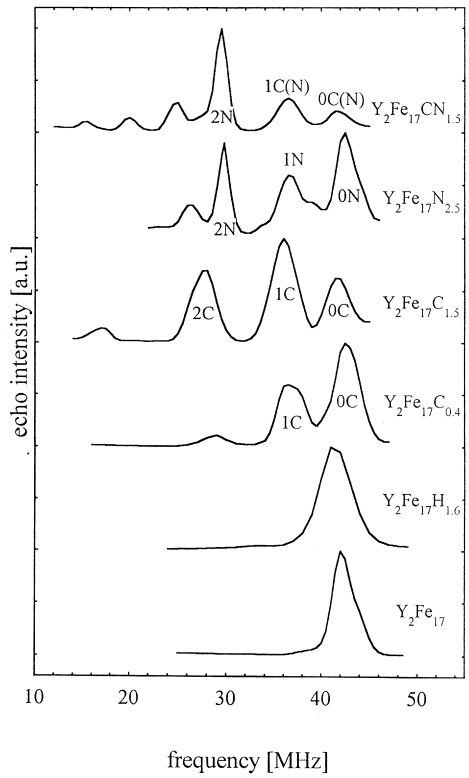

Fig. 2. ^{89}Y spin-echo NMR spectra of $Y_2Fe_{17}A_x$ (A=C,N,H) at 4.2 K (after Ref. [22]).

three well resolved satellite lines, in addition to the ^{89}Y ($I=1/2$ – no quadrupole splitting) line of the host compound. The lines at 42, 37, 29 and 17 MHz were assigned to the Y sites with 0, 1, 2 and 3 C atoms, respectively. A comparison of the corresponding B_e values shows that for the 1C configuration B_e is reduced by 12% with respect to the value for Y_2Fe_{17}. For the 2C and 3C environments it is reduced by 31 and 60%, respectively. As B_e for yttrium largely originates from transferred hyperfine fields, there must be a large C NN influence on the valence electron distribution and polarisation at the RE site. Note that recent inelastic neutron scattering measurements have shown similar reductions of the molecular field coefficient n_{Gd-Fe} caused by one or two carbon atoms neighbouring a Gd atom [23,24]. The reduction was found to be 12 and 29% for Gd sites with 1C and 2C neighbours, respectively. The main contribution to n_{RE-Fe} in these materials has been associated with the RE 5d electrons and with polarisation via 3d–5d hybridisation [25]. The transferred HFF on the RE nucleus has been found to arise mainly from polarisation of the 6s and 5d valence electrons (Y 5s and 4d, respectively) [26]. The almost identical changes in the transferred hyperfine field and in the molecular field coefficient showed the same reduction ratio for 6s and 5d (Y 5s and 4d) electron polarisation. A significant reduction of the molecular field coefficient n_{RE-Fe} has also been observed in magnetic measurements of the nitrides [27]. It corresponds to the reduction of transferred HFF at the RE sites caused by nitrogen neighbours [22]. Thus, the reduction of transferred HFF reflects a decrease of n_{RE-Fe}, caused by neighbouring carbon or nitrogen atoms.

^{89}Y NMR measurements of $Y_2Fe_{17}N_x$ have been reported [22,28]. Ref. [22] reports the ^{89}Y spectra of four samples prepared by heating Y_2Fe_{17} powder in a N_2 atmosphere. The amount of absorbed nitrogen x was estimated from the pressure difference before and after the reaction for the first three samples. With increasing reaction time between subsequent samples, approximate values of $x=0.5$, 1.2 and 2.5 were obtained. However, the distribution of nitrogen was found to be nonuniform, as discussed below. The ^{89}Y spectrum of $Y_2Fe_{17}N_{2.5}$ (Fig. 2) consists of four resonance lines: the main line at 42 MHz and lines at 36, 30 and 26 MHz, respectively. As for the carbon-containing compounds, the 36, 30 and 26 MHz lines have been assigned to Y atoms with 1N, 2N and 3N atoms as NNs, respectively. The set including 1N, 2N and 3N lines has been found to increase in intensity with x with respect to the 0N line. The intensity ratio within the set, however, remained unchanged, reflecting the growth of the nitrided outer shells of the grains. As shown by X-ray diffraction, the samples contained both the expanded nitride phase and the unnitrided phase. Most of the 0N intensity can therefore be attributed to the unnitrided cores of the grains. The intensity of the 2N line is the largest and the relative intensities within the set of 1N, 2N and 3N

lines are approximately constant with x. This indicates that, during the growth of the nitrided outer shell, the nitrogen concentration was approximately constant, with $2<x<2.5$. A similar set of samples has been treated by regrinding and subsequently vacuum annealing [28]. The ^{89}Y spectra did not show any changes in the distribution of nitrogen, which indicates that intermediate nitrogen concentrations could not be obtained. However, some authors have reported the existence of phases with intermediate nitrogen content $0<x<x_{max}$ for Sm_2Fe_{17} nitrides based on the results of X-ray diffraction [17], a.c. susceptibility, [29] and electron microscopy studies [30]. The results of a samarium NMR study of Sm_2Fe_{17} nitrides [31] confirm this finding, as will be discussed in more detail in the next paragraph. It indicates that the critical temperature for the formation of solutions with a continuous range of nitrogen concentration is lower for the samarium compound than for the yttrium compound and is possibly dependent on structural factors such as the lattice constants and the rare earth atom volume.

4.2. ^{147}Sm and ^{149}Sm resonances

Sm_2Fe_{17} possesses a planar anisotropy due to the anisotropy of the Fe sublattice which overcomes the preference of the Sm sublattice to align along the c-axis. The introduction of nitrogen gives rise to a dramatic increase of the CEF potential at the Sm site, leading to a strong enhancement of the anisotropy of the samarium sublattice. This results in the large uniaxial magnetic anisotropy of $Sm_2Fe_{17}N_x$ making it suitable for permanent magnet application. NMR measurements of samples prepared with nitrogen concentrations in the range $0<x<3$ were reported in Refs. [31,32]. The ^{147}Sm spectra of $Sm_2Fe_{17}N_x$, $x=0$, 0.4 and 2.5, samples are shown in Fig. 3. The ^{149}Sm and ^{147}Sm spectra were found to be consistent with each other. The sets of quadrupole septets ($I=7/2$ for both isotopes) have been assigned to Sm 6c sites with different numbers of nitrogen neighbours. The main septet for $x=0.4$ was assigned to Sm with 0N; the change of its quadrupole splitting with respect to Sm_2Fe_{17} could be ascribed to the change of easy magnetisation direction (EMD). The septet in the fully nitrided sample with $x=2.5$, possibly about 20% underestimated, was assigned to Sm with 3N neighbours. The slight change of HFF with magnetic moment direction for the 0N site indicates that Sm preserves its fully polarised state with $J_z = J = 5/2$. As the lattice EFG at the 0N site is axially symmetric with V_{zz} along the c-axis, Laplace's equation could be applied. V_{zz}(4f) and the c-axis component, V_{cc}(latt), could be obtained using V_{ii} for Sm_2Fe_{17} (c-plane) and for the 0N septet of the nitrided samples (c-axis) in Eq. (5). For 0N sites a V_{cc}(latt) value of 26×10^{20} V m^{-2} was obtained, and for 3N environments V_{cc}(latt) as large as 122×10^{20} V m^{-2} was derived. The latter value agrees,

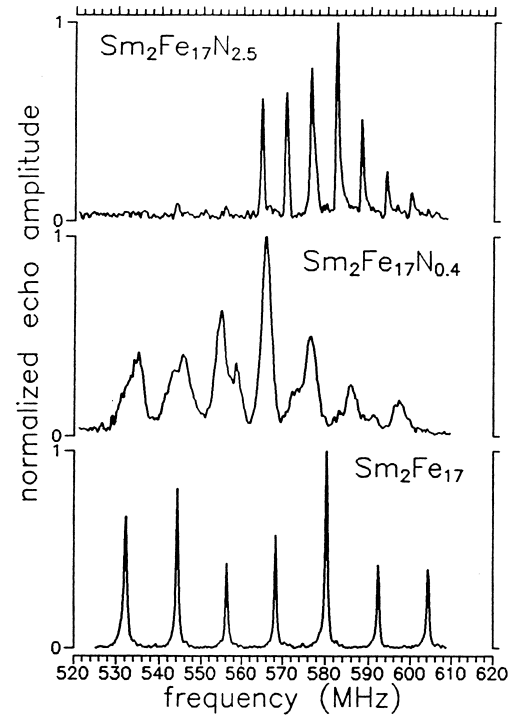

Fig. 3. ^{147}Sm spin-echo NMR spectra of $Sm_2Fe_{17}N_x$ at 4.2 K (after Refs. [31,32]).

within experimental error, with Gd Mössbauer measurements for $Gd_2Fe_{17}N_x$, V_{cc}(latt) $=126\times10^{20}$ V m^{-2} [33]. For V_{zz}(4f) a value of -249×10^{20} V m^{-2} was obtained, about 20% larger than the absolute value of 211×10^{20} V m^{-2} derived from an atomic beam experiment [34]. The HFF on Sm nuclei is dominated by a huge orbital contribution from 4f electrons. The transferred HFF is of opposite sign, so the higher HFF for Sm with nitrogen neighbours corresponds to a smaller transferred HFF, similarly to the effect found for $Y_2Fe_{17}N_x$ (Section 4.1).

The ^{147}Sm and ^{149}Sm NMR spin-echo spectra and the spin-echo decays of $Sm_2Fe_{17}C_x$, $x=0$, 0.5, 1 and 3, are reported in Ref. [35]. Carbides $Sm_2Fe_{17}C_x$ with $x=0.5$ and 1 were prepared by arc melting and the carbide with x close to 3 was prepared by heating a fine powder of Sm_2Fe_{17} in acetylene. These samples, together with a Sm_2Fe_{17} sample, were measured. Similar changes in the Sm spectra to those for the nitrides have been observed upon carbon uptake. A change of quadrupole splitting of the 0C septet between Sm_2Fe_{17} and $Sm_2Fe_{17}C_{0.5}$ has been attributed to the change of EMD between the compounds. A conical magnetic structure was found for $Sm_2Fe_{17}C_{0.5}$ at 4.2 K, with the EMD slightly tilted from the c-axis, similarly to $Sm_2Fe_{17}N_{0.4}$ [31]. The quadrupole splitting of the 3C septet corresponds to a V_{cc}(latt) of 137×10^{20} V m^{-2}. Relating V_{cc}(latt) and A_2^0 as in Section 3, a value of $-350\,Ka_0^{-2}$ was obtained for the 3C site. From the value of V_{cc}(latt) $=122\times10^{20}$ V m^{-2}, a corresponding value for A_2^0 of $-309\,Ka_0^{-2}$ was derived for the 3 N sites of $Sm_2Fe_{17}N_x$. This is smaller in magnitude than for the

3C sites in the carbides, implying that the hypothetical $Sm_2Fe_{17}C_3$ would have a larger magnetocrystalline anisotropy than $Sm_2Fe_{17}N_3$.

4.3. ^{143}Nd and ^{145}Nd resonances

The ^{145}Nd and ^{143}Nd NMR spin-echo spectra of Nd_2Co_{17} are reported in Ref. [36]. Central frequencies of 563 and 905 MHz were obtained, respectively. A quadrupole splitting of 7 MHz was derived for ^{143}Nd. The ^{145}Nd and ^{143}Nd NMR spin-echo spectra and echo decays for Nd_2Co_{17} and its interstitial nitride, $Nd_2Co_{17}N_3$, and hydride, $Nd_2Co_{17}H_{3.6}$, are reported in Ref. [37]. The ^{145}Nd spectrum of Nd_2Co_{17} (Fig. 4) shows a well resolved septet corresponding to a single Nd site 6c. The quadrupole splitting and the HFF were found to be 3.88 MHz and 391.7 T (central frequency 563.7 MHz), respectively. In the spectrum of the hydride the linewidths are much larger than in the host Nd_2Co_{17} and two septets can be distinguished. The overall quadrupole splitting determined from the line spacing is 3.8 MHz and B_e values of 391.7 and 389.3 T (central frequencies 563.7 and 560.0 MHz, respectively) are obtained. The ^{145}Nd spin-echo decays show characteristic oscillations caused by quadrupole interactions [38]. The oscillation period τ_q is related to the quadrupole splitting ν_q by the equation $\nu_q\tau_q = 1$, giving $\nu_q = 3.66$ MHz for the hydride. This value is similar to that

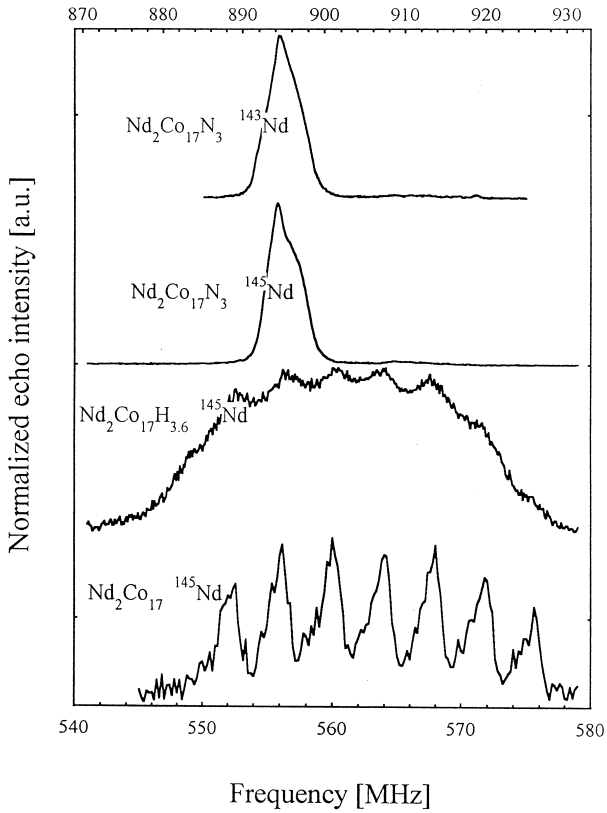

Fig. 4. ^{145}Nd and ^{143}Nd spin-echo NMR spectra of $Nd_2Co_{17}A_x$ (A = N,H) at 4.2 K (after Ref. [37]). The top frequency scale corresponds to ^{143}Nd.

obtained from the line spacing. A nonmonotonic decay of the oscillations indicates the presence of two quadrupole frequencies of very similar values, corresponding to the presence of two septets in the spectrum. Assuming that 3 H atoms per f.u. occupy 9e sites and 0.6 H enter the two 18g sites, as with $Nd_2Fe_{17}H_x$, and using the binomial distribution function, probabilities of 0.49, 0.42 and 0.09 for 0, 1 and 2 H 18g atoms as the NN to a Nd site were obtained. Therefore, the upper septet has been assigned to the Nd sites with 3H 9e neighbours and the lower septet has been attributed to the Nd sites with 3H 9e and 1H 18g sites. Thus, it is deduced that hydrogen influences the Nd hyperfine parameters, possibly when it occupies the 18g NN site. The decrease in the quadrupole splitting and B_e amount to 0.1–0.2 MHz and 2.4 T, respectively. The significant influence of H 18g and the slight influence of H 9e on HFF and the lattice EFG can be explained in terms of the strength of the bonding effects being strongly distance dependent. According to the above results the influence of H on the RE 5d and 6p electron population becomes apparent for a Nd–H(18g) distance of 2.35 Å, but is negligible for a Nd–H(9e) separation of 2.5 Å, similarly to that observed in $Sm_2Fe_{17}H_x$ [39].

A single unresolved line was obtained for both Nd isotopes in $Nd_2Co_{17}N_3$, corresponding to a B_e of 386.4 T. The values of ν_q determined from the quadrupole oscillations of spin-echo decays were 0.37 and 0.71 MHz for ^{145}Nd and ^{143}Nd, respectively, which correspond to an EFG component along the hyperfine field direction, V_{ii}, of 8.7×10^{20} V m^{-2}. The easy magnetisation direction in the host compound, the hydride and the nitride, as with the Fe-based compounds, lies in the *c*-plane. Similarly to the analysis for Sm compounds, the difference of EFG between the nitride and the host Nd_2Co_{17} of -82×10^{20} Vm^{-2} could be attributed mainly to the influence of the nitrogen NN atoms. This leads to a value of the increase of the *c*-axis component, ΔV_{cc}^{3N}(latt), of 164×10^{20} V m^{-2}. A corresponding value of 149×10^{20} V m^{-2} has been derived from a Gd Mössbauer study of $Gd_2Co_{17}N_x$ [40]. Relating the above V_{cc}^{3N}(latt) to A_2^0 gives a value as large as $-416\,Ka_0^{-2}$ for Nd sites with three nitrogen atoms as NN. This is about 50% greater in magnitude than for the isostructural Fe-based compound $Nd_2Fe_{17}N_x$ [41].

5. Sm_2Fe_{17}-based materials for permanent magnet technology

A study of the NMR spectra of ^{147}Sm and ^{149}Sm in Sm_2Fe_{17} powders nitrided under different conditions in NH_3 and N_2 has been reported in Ref. [42]. From the variations in the intensity of the septets on annealing in helium, the changes of nitrogen distribution and the domain wall structure were deduced. The 0N septet which appears in some samples nitrided for a short time revealed

the presence of unnitrided material. The quadrupole splitting of this septet revealed that, in the samples nitrided for a short time, the unnitrided phase had its EMD in the basal plane, whereas in the samples nitrided for a long time it was along the *c*-axis. As little as 1% unnitrided material can be detected using NMR. Thus, the sensitivity of the NMR technique to the amount of unnitrided phase is an order of magnitude higher than the X-ray or TMA techniques. The application of a 7 T field had no effect on the zero field Sm NMR signal of fine milled nitrided powders. This result indicates that the domain walls at the interface with unnitrided regions were not removed, even in such high fields.

A ^{57}Fe, ^{93}Nb, ^{147}Sm and ^{149}Sm nuclear magnetic resonance study of powders based on Sm_2Fe_{17} with 0, 4 and 10% Nb additions, and their nitrides, has been reported in Ref. [43]. The addition of Nb suppresses the formation of α-Fe, a phase which deteriorates the coercivity [44]. Spin-echo NMR spectra at zero applied field and the echo decays were measured in order to determine the sites of the elements in various phases of the materials. Two observed ^{93}Nb resonances were identified, corresponding to Nb in α-Fe and Nb in the 2:17 phase. The presence of Nb in the majority 2:17 phase was also found to be reflected in the linewidths and quadrupole splittings of the samarium spectra. The quantity of niobium entering the 2:17 phase was dependent on the amount of Nb added. This confirms the results of recent magnetic and metallographic studies [44,45]. The lowest Nb content in the 2:17 phase was found for a sample prepared using a HDDR route, which is consistent with Ref. [46].

From the intensities of the corresponding ^{57}Fe and ^{93}Nb lines the amount of α-Fe was estimated at 0.5–0.7% with an accuracy as high as 0.1%. A strong decrease of the Nb signal in α-Fe, together with a shift of the corresponding ^{57}Fe line to lower frequencies observed upon nitriding, was attributed to the occupation by nitrogen of the sites adjacent to Nb atoms. The results were found to be consistent with those obtained for Nb-free Sm_2Fe_{17} material and with the metallographic and magnetic data [44,45].

6. $RE_2TM_{14}B$

The compounds crystallise in a tetragonal structure (space group $P4_2/mnm$) [47] with two inequivalent rare earth sites, 4f and 4g. The 4f site has two B and two RE NN atoms, whereas the 4g site has a single B and three RE NN. Both sites have the same number of 3d neighbours. There are six inequivalent Fe sites: c, e, j_1, j_2, k_1 and k_2. The crystallographic, magnetic and material properties of $RE_2TM_{14}B$ have recently been reviewed in Ref. [48].

The ^{139}La spin-echo spectra of $La_2Fe_{14}B$ have been reported in Ref. [49] (Fig. 5). Since lanthanum has the $4f^0$ configuration, the 4f electron contributions to the HFF and

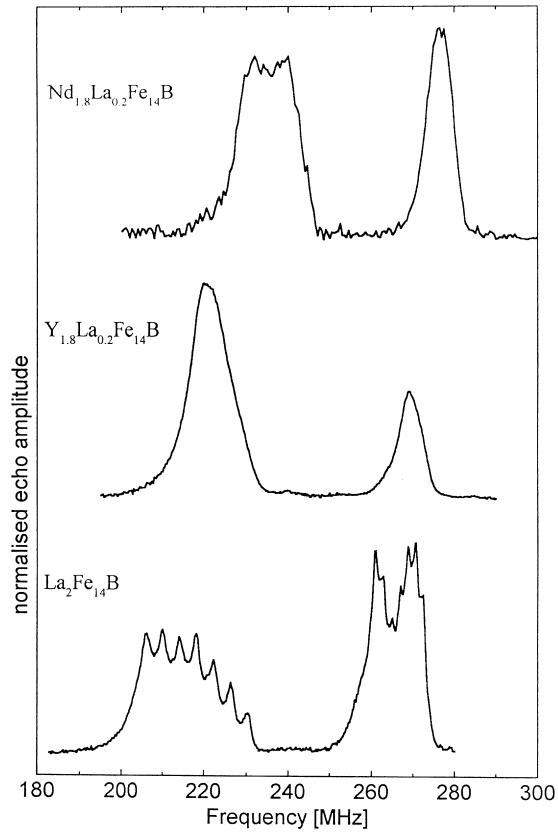

Fig. 5. ^{139}La spin-echo NMR spectra of $La_2Fe_{14}B$, $La_{0.2}Nd_{1.8}Fe_{14}B$ and $La_{0.2}Y_{1.8}Fe_{14}B$ at 4.2 K (after Ref. [49]).

EFG vanish, giving the opportunity for an accurate determination of the lattice EFG and transferred HFF at the 4f and 4g crystallographic sites. Similar V_{cc}(latt) and A_2^0 values for both sites were found from Gd Mössbauer measurements [50], as from the theoretical calculations for $Gd_2Fe_{14}B$ [7]. However, both values differed by a factor of more than 2 for Sm and Nd NMR in $Sm_2Fe_{14}B$ and $Nd_2Fe_{14}B$ [51]. As the EMD for $La_2Fe_{14}B$ is the *c*-axis, the quadrupole splitting corresponds directly with V_{cc}(latt). Following the theoretical calculations of the ''transferred'' HFF [26] the upper septet is assigned to the 4f site and the lower septet to the 4g site. The corresponding B_e are 36.1 T for the 4g and 44.1 T for the 4f site.

The values of the quadrupole splittings are 4.05 MHz for the 4g and 1.93 MHz for the 4f site, indicating that V_{cc}(latt) and thus A_2^0 of the 4g site is more than two times larger than that of the 4f site. In Ref. [52] an average value of $330\,Ka_0^{-2}$ was obtained from magnetic measurements, whereas in Ref. [53] different values for A_2^0 of $136\,Ka_0^{-2}$ for the 4f site and $190\,Ka_0^{-2}$ for the 4g site were derived from analysis of the spin structure of the compounds. Recent theoretical FLMTO calculations have given similar V_{cc}(latt) values for both sites [54]. Thus, the question arises concerning errors in the calculation of EFG with this newest computational method.

On the basis of the EFG values obtained from NMR it

was concluded that the lowest order contribution to the CEF at the 4g site is about two times larger than from the 4f site. The FLMTO calculations [54] led to A_2^0 values of $476\,Ka_0^{-2}$ for the 4g and $284\,Ka_0^{-2}$ for the 4f site with a ratio of 1.7, which is close to that derived from NMR.

A strong line intensity corresponding to the 4g site was observed in the spectra of ^{139}La for samples $La_{0.2}Nd_{1.8}Fe_{14}B$ and $La_{0.2}Y_{1.8}Fe_{14}B$ (10% La substitution) [49] (Fig. 5). The ratio of the area under the 4g and 4f peak was found to be 1.8 for the Nd and 3.7 for the Y sample. These values are a measure of the ratio of lanthanum occupancy at the 4g and 4f sites. The larger ratio for the Y sample is in agreement with the prediction based on the difference of the atomic radii. This difference is larger for La and Y than for La and Nd. The measurement on $La_{0.1}Y_{1.9}Fe_{14}B$ (corresponding to 5% La substituted for Y) gives a ratio of 3.9. This is larger than for the sample with 10% La, i.e. at a low substituent content the deviation from a random distribution is larger than for the more substituted sample.

7. Conclusions

Frequency-swept spin-echo NMR allows the accurate determination of hyperfine fields and electric field gradients at individual sites. The nuclei of most elements can serve as NMR probes and the resolution is generally higher than in Mössbauer measurements. Recent developments in the construction of untuned, computer controlled NMR spectrometers has made the experiments much more effective.

The local influence of the neighbouring atoms on HFF and EFG can be studied with high accuracy owing to their impact on the valence electrons of the probe atom. These features enable the determination of the content and distribution of interstitial elements at the various atomic sites. They also allow the phases present in the material to be distinguished and provide an ideal tool to study the effects of substitution or doping with sensitivity, which is often impossible to achieve by other experimental techniques.

The values of the EFG at individual sites are a source of information on the spectroscopic state of the rare earth sites and can be used to ascertain the origin of the magnetocrystalline anisotropy and to determine the contributions of the individual sites to it. This, together with information on the distribution of elements over atomic sites, is vital for a correct description of the magnetic and anisotropic properties of magnetic materials such as $Nd_2Fe_{14}B$ with rare earth substitution.

Measurements of nuclear relaxation times, power dependence and the changes in behaviour under applied magnetic fields are helpful in the determination of the origin of the NMR signal. These measurements make it possible to distinguish between the domain wall centre and domain wall edge signals, enabling a reliable and comprehensive interpretation of the NMR results to be made.

The significant enhancement of the NMR signal, especially large for low anisotropy materials, and the high resolution of the method enable a very accurate comparative determination of the amounts of spurious soft magnetic phases such as α-Fe or unnitrided Sm_2Fe_{17}. Such information can be applied to optimise the technological routes of magnet processing for specific end products.

Acknowledgements

The author gratefully acknowledges collaboration with Prof. P.C. Riedi, M. Rosenberg, H. Figiel and K.H.J. Buschow.

References

[1] A. Abragam, The Principles of Nuclear Magnetism, Clarendon Press, Oxford, 1961.
[2] E. Fukushima, S.B.W. Roeder, Experimental Pulse NMR, Addison-Wesley, Reading, Massachussets, 1981.
[3] A.M. Portis, R.H. Lindquist, in: G.T. Rado, H. Suhl (Eds.), Magnetism, Vol. IIA, Academic Press, New York, 1965, p. 357.
[4] M.A.H. McCausland, I.S. Mackenzie, Adv. Phys. 28 (1979); Nuclear Resonance in Rare Earth Metals, Taylor and Francis, London, 1980.
[5] P.C. Riedi, in: A.P. Cracknell, R.A. Vaughan (Eds.), Magnetism in Solids, SUSSP, Edinburgh, 1981, p. 445.
[6] H. Figiel, Magn. Res. Rev. 16 (1991) 101.
[7] R. Coehoorn, K.H.J. Buschow, J. Appl. Phys. 6 (1991) 5590.
[8] J.S. Lord, P.C. Riedi, Meas. Sci. Technol. 6 (1995) 149.
[9] E. Gratz, A. Lindbaum, A.S. Markosyan, H. Mueller, A.Yu. Sokolov, J. Phys.: Condensed Matter 6 (1994) 6699.
[10] S. Hirosawa, Y. Nakamura, J. Magn. Magn. Mater. 25 (1982) 284.
[11] C. Kapusta, I.S. Oliveira, P.C. Riedi, E. Gratz, G. Wiesinger, H. Figiel, A.P. Guimarâes, J. Magn. Magn. Mater. 177–181 (1998) 1121.
[12] C. Kapusta, P.C. Riedi, K.H.J. Buschow, J. Alloys Comp. 198 (1993) 59.
[13] P.C.M. Gubbens, A.M. van der Kraan, K.H.J. Buschow, Hyperfine Interactions 53 (1989) 37.
[14] R.B. Helmholdt, K.H.J. Buschow, J. Less-Common Met. 155 (1989) 15.
[15] O. Isnard, J.L. Soubeyroux, S. Miraglia, D. Fruchart, L.M. Garcia, J. Bartolome, Physica B 180 (1992) 629.
[16] O. Isnard, S. Miraglia, J.L. Soubeyroux, D. Fruchart, L. Pannetier, Phys. Rev. B 45 (1992) 2920.
[17] S. Brennan, R. Skomski, J.M.D. Coey, IEEE Trans. Magn. 30 (1994) 571.
[18] Y.N. Wei, K. Sun, Y.B. Fen, Y.X. Zhang, B.P. Hu, Y.Z. Wang, X.L. Rao, G.C. Liu, J. Alloys Comp. 194 (1993) 9.
[19] Q.W. Yan, P.L. Zhang, Y.N. Wei, K. Sun, B.P. Hu, Y.Z. Wang, G.C. Lui, C. Gau, Y.F. Cheng, Phys. Rev. B 48 (1993) 2878.
[20] C.N. Christodoulou, T. Takeshita, J. Alloys Comp. 198 (1993) 1.
[21] H. Fujii, H. Sun, in: K.H.J. Buschow (Ed.), Handbook of Magnetic Materials, Vol. 9, Elsevier, Amsterdam, 1995, p. 303.
[22] C. Kapusta, M. Rosenberg, J. Zukrowski, H. Figiel, T.H. Jacobs, K.H.J. Buschow, J. Less-Common Met. 171 (1991) 101.

[23] M. Loewenhaupt, P. Tils, K.H.J. Buschow, R.S. Eccleston, J. Alloys Comp. 222 (1995) 39.
[24] M. Loewenhaupt, P. Tils, K.H.J. Buschow, R.S. Eccleston, J. Magn. Magn. Mater. 152 (1996) 10.
[25] M.S.S. Brooks, O. Eriksson, B. Johansson, J. Phys.: Condensed Matter 1 (1989) 5861.
[26] R. Coehoorn, K.H.J. Buschow, J. Magn. Magn. Mater. 118 (1993) 175.
[27] K.H.J. Buschow, R. Coehoorn, D.B. DeMooij, K. DeWaard, T.H. Jacobs, J. Magn. Magn. Mater. 92 (1990) L35.
[28] Y.D. Zhang, J.I. Budnick, D.P. Yang, G.W. Fernando, W.A. Hines, T.D. Xiao, T. Manzur, Phys. Rev. B 51 (1995) 12091.
[29] M. Katter, J. Wecker, C. Kuhrt, L. Schultz, R. Grössinger, J. Magn. Magn. Mater. 117 (1992) 419.
[30] D.S. Edgley, B. Saje, A.E. Platts, I.R. Harris, J. Magn. Magn. Mater. 138 (1994) 6.
[31] C. Kapusta, M. Rosenberg, P.C. Riedi, M. Katter, L. Schultz, J. Magn. Magn. Mater. 134 (1994) 106.
[32] C. Kapusta, M. Rosenberg, R.G. Graham, P.C. Riedi, T.H. Jacobs, K.H.J. Buschow, J. Magn. Magn. Mater. 104 (1992) 1333.
[33] M.W. Dirken, R.C. Thiel, R. Coehoorn, T.H. Jacobs, K.H.J. Buschow, J. Magn. Magn. Mater. 94 (1991) 415.
[34] B. Bleaney, in: J.R. Elliot (Ed.), Magnetic Properties of Rare Earth Metals, Plenum Press, New York, 1972, chapt. 8.
[35] C. Kapusta, P.C. Riedi, J.S. Lord, R. Mycielski, K.H.J. Buschow, J. Alloys Comp. 235 (1996) 66.
[36] R.L. Streever, Phys. Rev. B 16 (1977) 1796.
[37] C. Kapusta, P.C. Riedi, R. Mycielski, G.J. Tomka, J. Appl. Phys. 81 (1997) 4563.
[38] H. Abe, H. Yasuoka, A. Hirai, J. Phys. Soc. Jpn. 21 (1966) 77.
[39] C. Kapusta, J.S. Lord, P.C. Riedi, J. Magn. Magn. Mater. 159 (1996) 207.
[40] F.M. Mulder, R.C. Thiel, R. Coehoorn, T.H. Jacobs, K.H.J. Buschow, J. Magn. Magn. Mater. 117 (1992) 413.
[41] C. Kapusta, J.S. Lord, P.C. Riedi, K.H.J. Buschow, J. Alloys Comp. 221 (1995) 105.
[42] C. Kapusta, P.C. Riedi, G.J. Tomka, W. Kocemba, S. Brennan, J.M.D. Coey, in: F.P. Missell, V. Villas-Boas, H.R. Rechenberg, F.J.G. Landgraf (Eds.), Proceedings of the IX International Symposium on Magnetic Anisotropy and Coercivity in Rare Earth Transition Metal Alloys, Sao Paulo, 1996, World Scientific, Singapore, 1996, p. 217.
[43] C. Kapusta, P.C. Riedi, G.J. Tomka, R. Mycielski, B. Saje, S.A. Sinan, I.R. Harris, in: F.P. Missell, V. Villas-Boas, H.R. Rechenberg, F.J.G. Landgraf (Eds.), Proceedings of the IX International Symposium on Magnetic Anisotropy and Coercivity in Rare Earth Transition Metal Alloys, Sao Paulo, 1996, World Scientific, Singapore, 1996, p. 327.
[44] A.E. Platts, I.R. Harris, J.M.D. Coey, J. Alloys Comp. 185 (1992) 251.
[45] S.A. Sinan, D.S. Edgley, I.R. Harris, J. Alloys Comp. 226 (1995) 170.
[46] O. Gutfleisch, J.C. Clarke, A.C. Neiva, S.A. Sinan, I.R. Harris, J. Alloys Comp. 233 (1996) 139.
[47] J.F. Herbst, J.J. Croat, F.E. Pinkerton, W.B. Yelon, Phys. Rev. B 29 (1984) 4176.
[48] J.F. Herbst, Rev. Mod. Phys. 63 (1991) 819.
[49] C. Kapusta, J. Magn. Magn. Mater. 157–158 (1996) 71.
[50] M. Bogé, G. Czjzek, D. Givord, C. Jeandey, H.S. Li, J.L. Oddou, J. Phys. F: Met. Phys. 16 (1986) L67.
[51] C. Kapusta, H. Figiel, G. Stoch, J.S. Lord, P.C. Riedi, IEEE Trans. Magn. 29 (1993) 2893.
[52] R.J. Radwanski, J.J.M. Franse, J. Magn. Magn. Mater. 83 (1990) 151.
[53] M. Yamada, Y. Yamaguchi, H. Kato, H. Yamamoto, Y. Nakagawa, S. Hirosawa, M. Sagawa, Solid State Commun. 56 (1985) 663.
[54] K. Hummler, M. Fähnle, Phys. Rev. B 53 (1996) 3290.